Research Article *http://dx.doi.org/10.4314/mejs.v15i2.8*

Structural, Dielectric, Complex Impedance and Magnetoelectric Properties of the (1-x) $KNbO_3$ - x$MgFe_2O_4$ Composites

Tesfakiros Woldu*
Department of Physics, Mekelle University, P.O.Box 231, Mekelle, Tigray, Ethiopia (*tepsikir@gmail.com).

ABSTRACT

Ferrite-ferroelectric nanoparticle composites have a promising potential for a wider range of applications for the manufacturing of new-generation devices due to the tenability of their electric and magnetic orders. In this present work, room-temperature magnetoelectric (ME) coupling studies of KNbO3/MgFe2O4 composites having a general formula (1-x) KNbO3 - xMgFe2O4 (where x = 0, 0.1, 0.3, 0.5, 0.7, 0.9, 1) is presented. The presence of the cubic spinel-ferrite phase of MgFe2O4 and the orthorhombic ferroelectric phase of KNbO3 were confirmed by the structural analysis which was employed using X-ray diffraction (XRD), Raman spectroscopy, and morphology and grain size using Transmission electron microscopy (TEM). Magnetization versus magnetic field (M-H) measurements conform to ferromagnetic ordering and show improved magnetization with the increase in the ferrite phase. The existence of coupling between ferroelectric and ferromagnetic ordering was performed using a lock-in amplifier ME measurement setup. All the composite samples show good linear magnetoelectric coupling that increases with increasing ferrite content. This composite nanostructure with a well-defined interface provides the possibility of an ideal model of room temperature ME coupling which is significant from the technological point of view for a variety of miniaturized next-generation device applications.

Keywords: Ferroelectric, Ferromagnetic, Multifferroic, Composite, Magnetoelectric coupling, Magneto-electric.

1. INTRODUCTION

Nowadays study on multiferroic materials that simultaneously display polarization, magnetization and ferroelastic ordering drastically increased not only for the underlying new physics but also for promising potential applications. The coexistence of both ferroelectric and ferromagnetic orders in the same material is predictable to create magneto-electric (ME) property due to the interaction between polarization and magnetization consequently, the coupling between electric and magnetic order occur. Magneto electric material with strong coupling between polarization and magnetization allows the ability to tune the electric property with the magnetic field and vice-versa (Raneesh et al., 2015). Magnetoelectric coupling effect has attracted significant interest due to its potential applications in new generation devices such as

Submitted on: 22nd May 2023 ***Revised and Accepted on: 18th June 2023***

sensors, nonvolatile data storages, actuators, and transducers (Kim et al., 2014; Eerenstein et al., 2006; Fiebig, 2015). There are only very few naturally existing single-phase materials that exhibit room-temperature magneto-electric properties that show strong coupling Hill (2000). Multiple-phase multiferroics that yield a giant extrinsic ME coupling effect at room temperature can be obtained by combining ferroelectric and ferromagnetic materials and coupling facilitated through piezoelectric and magnetostrictive elastic interactions (Ramesh et al, 2017; Spaladin et al 2005; Giorgio, 2013).

When an electric field is applied, to the piezoelectric phases its volume changes, and exerts a force against the ferromagnetic counterpart, latter the magnetostrictive with piezomagnetic phase also, in turn, develops magnetization as a result of mechanical strain. To improve coupling interaction through magnetic-piezoelectric phases, different connectivity patterns have been studied (Zhai et al., 2008; Ramesh et al, 2007; Nan et al., 2008).

ME response of a single-phase material is limited because, in most such materials, the origin of ferroelectricity and ferromagnetic order are largely unrelated, for example; $BiFeO_3$, $YMnO_3$, and $BaTiO_3$ to obtain such multiferroic single-phase compound with large and strong ferromagnetic and ferroelectric ordering is a challenge (Wang et al., 2009). But, this situation in the composite multiferroic magnetoelectric system is different, since the origin of magnetoelectric coupling lies at the interface between the magnetic and ferroelectric phases (Liu et al., 2013; Vaz et al, 2010). Except for problems of high leakage current that arises due to magnetic phases, thermal expansion difference, and grain boundary between the two phases ME composites yields extrinsic ME effect.

Recently, based on this idea a number of different bulk ME composites mainly ferrite-ferroelectric ceramics have been synthesized and investigated, such as $BaTiO_3$, PZT, $KNbO_3$, $Pb(MgNb)O_3$ etc. are usually chosen as ferroelectric phase, and $CoFe_2O_4$, $BiFeO_3$, $NiFe_2O_4$, Fe_3O_4 , $MgFe_2O_4$ usually chosen as magnetic phase (Ramesh et al., 2017; Petrov et al., 2007; Koo et al., 2009; Park et al., 2009; Corral et al., 2010; Zhao et al., 2014; Xie et al., 2011; Zhu et al., 2014; Tan et al., 2008; Raidongia et al., 2010; Nayek et al., 2013; Wang et al., 2002; Islam et al., 2008; Komalavalli et al., 2019).

In this study, $KNbO_3$ selected as ferroelectric material and $MgFe_2O_4$ as ferromagnetic material. $KNbO_3$ nanocrystalline powder synthesized using solid-state reaction and $MgFe_2O_4$ nanocrystalline powder using sol-gel method and the composites of $(1-x)KNbO_3$ - $xMgFe_2O_4$ (x

= 0, 0.1, 0.3, 0.5, 0.7, 0.9, 1) were prepared mixing $KNbO_3$ and $MgFe_2O_4$ nanocrystalline powders using solid-state reaction method with different molar fractions. The structural, dielectric, magnetic and magneto electric coupling of the synthesized composites were investigated.

2. METHODOLOGY

2.1. Synthesis

The (1-x) $KNbO_3$ - x$MgFe_2O_4$ (x = 0, 0.1, 0.3, 0.5, 0.7, 0.9, 1) composite samples were synthesized by three-step processes, sol-gel method to synthesize ($MgFe_2O_4$), conventional solid state reaction to synthesize ($KNbO_3$), and followed by solid state reaction to synthesize the composites. All the chemicals in analytic pure grade purchased. $MgFe_2O_4$ powder obtained from $Mg(NO_3)_2.6H_2O$, $Fe(NO_3)_3.9H_2O$, and PVA with a molecular weight of 125,000 was synthesized via PVA assisted sol-gel. $MgFe(NO_3)_2.6H_2O$ and $Fe(NO_3)_3.9H_2O$ dissolved separately (Mg: Fe=1:2) in distilled water. After constantly stirring for about 2 hrs, PVA was added. The combined solution heated to 60 ^{0}C and subjected to constant stirring until a gel was obtained. Then the precursor heated to 90 ^{0}C and calcined at 850 ^{0}C for 4 hrs finally $MgFe_2O_4$ nanoparticles obtained. $KNbO_3$ obtained by mixing $KHCO_3$ and Nb_2O_5 with Agate Mortar and Pestle on wet-ground in molar proportion for 4 hrs and then at 850 ^{0}C for 3 hrs. Composite ceramics samples prepared using conventional solid-state reaction method with weight fractions 10 %, 30 %, 50 %, 70 %, and 90 % of $MgFe_2O_4$ powder to 90 %, 70 %, 50 %, 30 %, and 10 % of $KNbO_3$ powder, sintered at a temperature of 850 ^{0}C for 5 hrs, and finally painted by silver paste for magnetoelectric coupling and dielectric spectroscopy measurements.

2.2. Measurnments

All the samples were analyzed by various techniques. Room temperature crystal structure of the samples was examined by using an X-ray diffractometer (*PANalytical, X'Pert PRO*) with a mono-chromatized Cu-K_α radiation (λ=1.54060 Å). The surface morphology, size and the local crystallographic structure were investigated by high-resolution transmission electron microscope (*HRTEM, JEOL-JEM 2100*) operating at 200kV. Raman measurements were performed at room temperature using the Jobin-Yvon T64000 triple spectrometer system, equipped with a confocal microscope and a nitrogen-cooled CCD detector. Dielectric measurements as a function of frequency between 100 Hz to 2 MHz were performed using an impedance analyzer (*Agilent*,

E4980A). Magnetic measurements were were conducted using vibrating sample magnetometer VSM (*Lake-shore* 7404) at applied field strength of ±3 kOe. The direct ME coupling coefficients of (1-x)$KNbO_3$ - x$MgFe_2O_4$ (where x = 0.1, 0.3, 0.5, 0.7, 0.9) is measured using magneto-electric coupling set up.

3. RESULT AND DISCUSSION

3.1. Structural and Morphology

The X-ray diffraction patterns of the individual ferroelectric $KNbO_3$ (KN) and ferromagnetic $MgFe_2O_4$ (MF), and (1-x)$KNbO_3$ - x$MgFe_2O_4$ (where x = 0, 0.1, 0.3, 0.5, 0.7, 0.9, 1) composite is shown in figure 1. The obtained XRD patterns of the composites clearly show both ferroelectric ($KNbO_3$) and ferromagnetic ($MgFe_2O_4$) phases XRD characteristics patterns. The XRD peaks positions and intensities with miller indices (101), (111), (202), (020), (212), (121), (022), (222), (402) and (131) are in correlation with the agreement reported in JCPDS files no. 71-2171 orthorhombic structure of $KNbO_3$. As seen in figure 1 the composites have been found in a highly pure phase. The XRD peaks positions and intensities with miller indices (220), (311), (200), (400), (422), (511), (440) and (533) are in correlation with the agreement reported in JCPDS files no. 71- 1232 spinel cubic crystal structure of $MgFe_2O_4$.

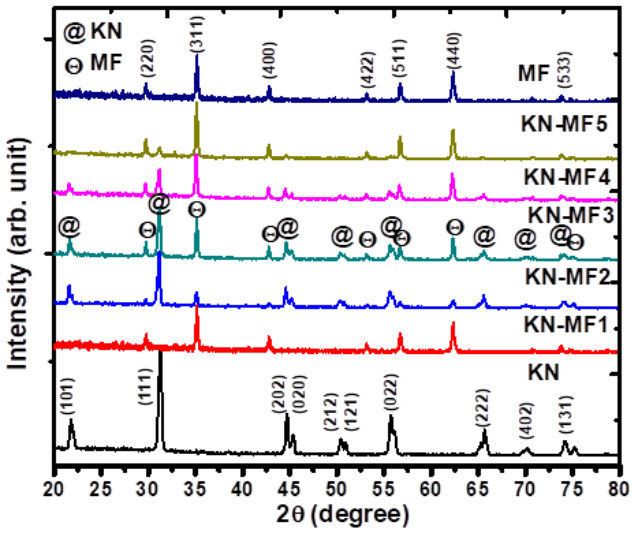

Figure 1. X-ray diffraction patterns of pure $KNbO_3$, $MgFe_2O_4$, and (1-x)$KNbO_3$ - x$MgFe_2O_4$ (where x = 0, 0.1, 0.3, 0.5, 0.7, 0.9, 1) composite.

Figure 2 shows room temperature Raman Spectra of pure $KNbO_3$ and $MgFe_2O_4$, and (1-x)$KNbO_3$ - x$MgFe_2O_4$ (where x = 0, 0.1, 0.3, 0.5, 0.7, 0.9, 1) composite recorded in the range

between 100 – 850 cm^{-1}. The significant five Raman-active modes ($A_{1g} + E_g + 3F_{2g}$) assigned for pure $MgFe_2O_4$ positioned at 217 cm^{-1}, 486 cm^{-1} and 554 cm^{-1} for F_{2g} modes; 333 cm^{-1} for E_g vibration and 646 cm^{-1} for and A_{1g} vibration are characteristic bands which are typical of the cubic inverse-spinel structure (Abraham et al., 2017). The significant Raman Active modes ($4A_1 + 4B_1 + 3B_2 + A_2$) assigned for pure $KNbO_3$ was carried out according to (Quittet et al., 1976; Sadhana et al., 2013).

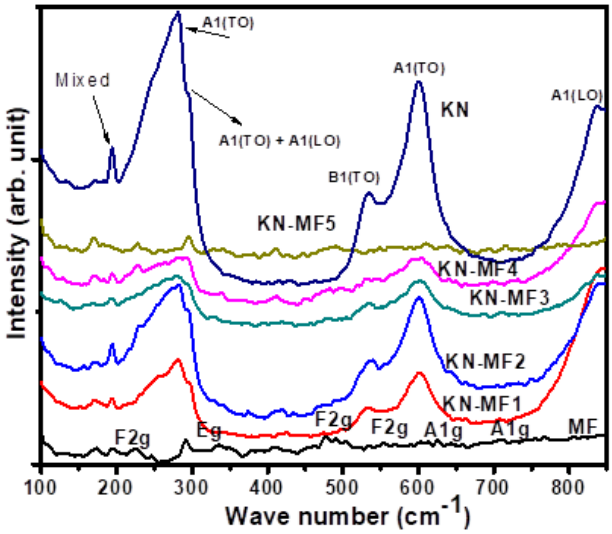

Figure 2. (1-x)$KNbO_3$ - x$MgFe_2O_4$ composites Raman Spectra.

Raman spectrum is characterized by low to mid-wave number region characterized by a broad A_1 (TO) mode centered at 270 cm^{-1}, fano-type interference dip at 195 cm^{-1} and two sharp modes at 192 cm^{-1} which is a mixed mode of vibrations due to B_1 (TO), A_1 (TO), A_1 (LO), and B_1 (TO) and modes at 296 cm^{-1} due to vibration of A_1 (LO) and A_1 (TO) modes. Modes at appeared merged as a single peak because of the resolution limit of the instrument (Shen et al., 1995). Raman active modes of higher wave-number regions (>500 cm^{-1}) are distinguished by A_1 (TO) mode at 596 cm^{-1}, and A_1(LO) at 834 cm^{-1} which are associated with octahedral vibration. Sample code and omposition of $KNbO_3$ and $MgFe_2O_4$ in each sample shown in table 1.

Table 1. Sample code and percentage of $KNbO_3$ and $MgFe_2O_4$ in each sample.

Sample code	***KN*** *(x=0)*	***KN-MF1*** *(x=0.1)*	***KN-MF2*** *(x=0.3)*	***KN-MF3*** *(x=0.5)*	***KN-MF4*** *(x=0.7)*	***KN-MF5*** *(x=0.9)*	***MF*** *(x=1)*
$KNbO_3$ (%)	100	90	70	50	30	10	0
$MgFe_2O_4$ (%)	0	10	30	50	70	90	100

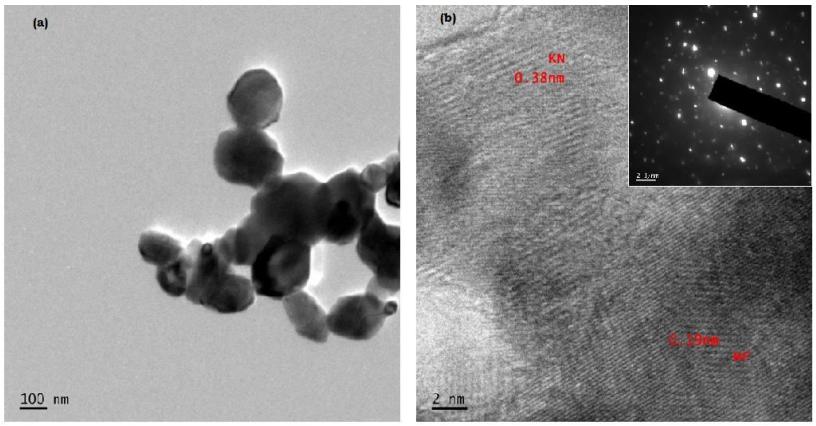

Figure 3. (a) TEM image and (b) HRTEM lattice pattern and the inset pattern SAED of KN-MF3 sample.

The morphology of KN-MF3 revealed by TEM images as shown in figure 3a. The HRTEM image clearly shows lattice fringe separations in the high-resolution image with 2 nm resolution and reveals the clear interface between ferrite MF and ferroelectric KN phases. The calculated interplanar distance (d-spacing) was 0.38 nm for KN and 0.19 nm for MF. The inset in figure 3(b) shows Selected area electron diffraction (SAED) pattern reveals the presence of ferrite MF and ferroelectric KN microstructures in the composite.

Chemical impurity and stoichiometry composite sample, KN-MF3 was confirmed using Energy Dispersive X-Ray Spectroscopy (EDX) as shown in figure 4. The EDX spectrum analysis over the entire spectrum range reveals the presence of elements Mg, Fe, O, K, Nb and O in KN-MF3 composite that shows strong peaks of K, Nb, Mg and Fe. The elemental composition and atomic concentration of KN-MF3 sample clearly shown in table 2.

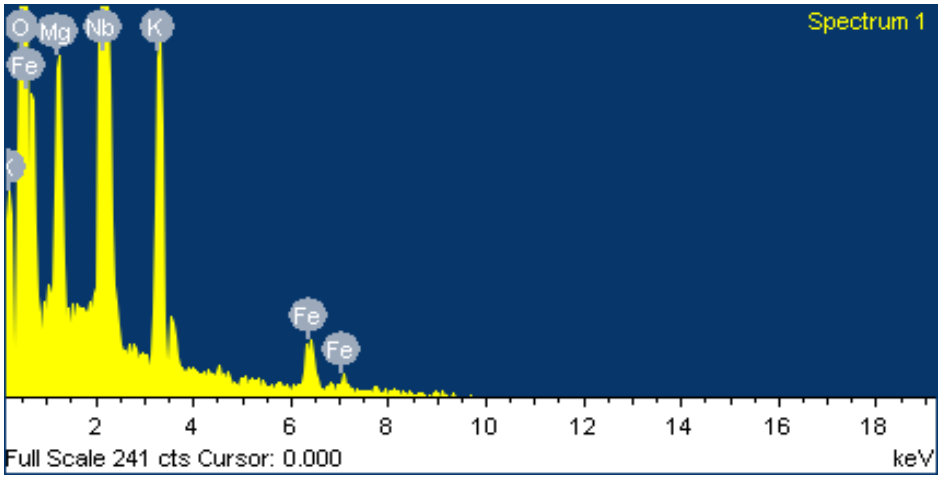

Figure 4. EDX Spectrum of sample KN-MF3.

Table 2. Elemental composition and atomic concentration of KN-MF3 sample.

Element	***Mg***	***O***	***K***	***Nb***	***Fe***	***Total***
Weight (%)	4.24	28.90	6.9	22.77	37.19	100
Atomic (%)	5.68	58.88	5.75	7.99	21.70	100

3.2 Dielectric Analysis

Dielectric characterization as a function of frequency between 100 – 2 MHz is performed by Impedance analyzer (*Agilent*, E4980A) at room temperature. Real dielectric constant (permittivity) of the samples is calculated using $\boldsymbol{\varepsilon' = \frac{cd}{\varepsilon_0 A}}$ (1)

Where, *c* is capacitance, *d* thickness of the pellet, *A* cross-sectional area, and ε_0 (permittivity of free space), $\varepsilon_0 = 8.85 \times 10^{-12} F/m$.

Imaginary dielectric constant (permittivity) was calculated using the relation $\varepsilon'' = \varepsilon' tan\delta$ (2)

AC conductivity (σ_{AC}) was calculated from the obtained dielectric data using the relation

$$\sigma_{AC} = \omega \varepsilon' \varepsilon_0 tan\delta = 2\pi f \varepsilon' \varepsilon_0 tan\delta \quad (3)$$

Where, ω is the angular frequency which is $2\pi f$

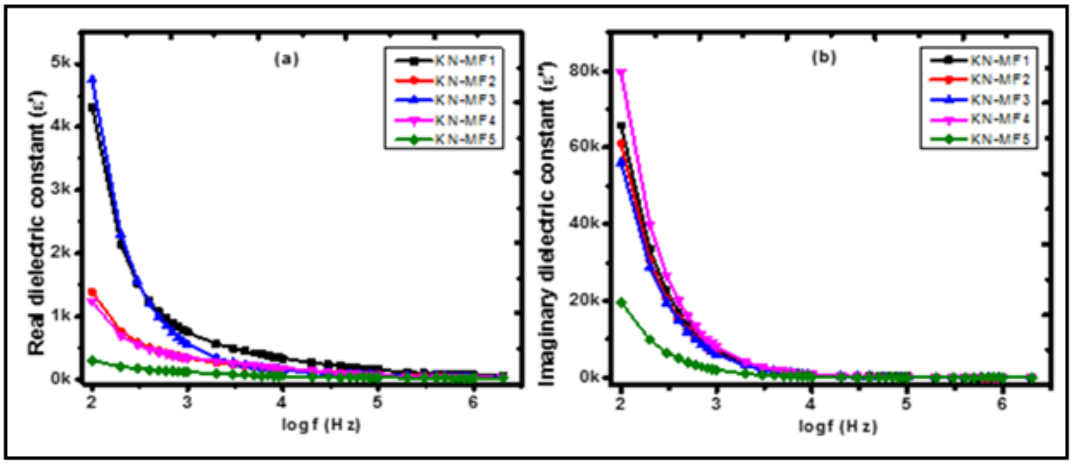

Figure 5. (a) Frequency dependence of real dielectric constant and (b) Frequency dependence of imaginary dielectric constant of (1-x)$KNbO_3$ - x$MgFe_2O_4$ mixed composites.

Figure 5(a) shows room temperature frequency dependence of real permittivity (ε') and figure 5(b) room temperature frequency dependence of imaginary dielectric constant (ε'') of (1-x)$KNbO_3$ - x$MgFe_2O_4$ mixed composites. All samples show a strong frequency dependence, at lower frequency have higher dielectric constant that decreases abruptly at lower frequency and have lower value/nearly constant at higher frequency as seen in figure 5(a) which is a common

behaviour of dielectric materials. At low frequency the high dielectric constant value of the composites attributed to the heterogeneity of composite structure that caused due to interfacial polarization.

The applied electric field induces ferrite phase to accumulate space charge at the interface of the two phases due to the presence of different permittivity and conductivity (Pascua-Gonzalez et al., 2016). At low frequency excitation of bound electrons, lattice vibration, dipole orientation and interfacial polarization (Rani et al., 2014) cause for dielectric constant to be maximum. This can be explained in terms of Maxwell-Wagner polarization and Koop's phenomenological theory of dielectrics (Pandya et al., 2015; Wagner, 1993) induced by a different dielectric constant at the interface as a result, overall polarization enhanced causing the rise of dielectric constant. At the higher frequency dielectric constant becomes very small because of the inability of electric dipoles to match the applied alternating electric field. Consequently, hopping of electrons between Fe^{2+} - Fe^{3+} in electronic polarization can't follow the applied electric field Koops (1951). It must be noted that the highest dielectric constant observed is for sample KN - MF1 sample which is a percolation limit due to the major contribution of interfacial polarization. A similar fashion was observed for imaginary dielectric constant versus frequency as seen in figure 5(b) except decreasing very fast with increasing frequency from 2 MHz to 3.5 MHz whereas real dielectric constant decreases relatively slowly from 2 MHz to 5 MHz.

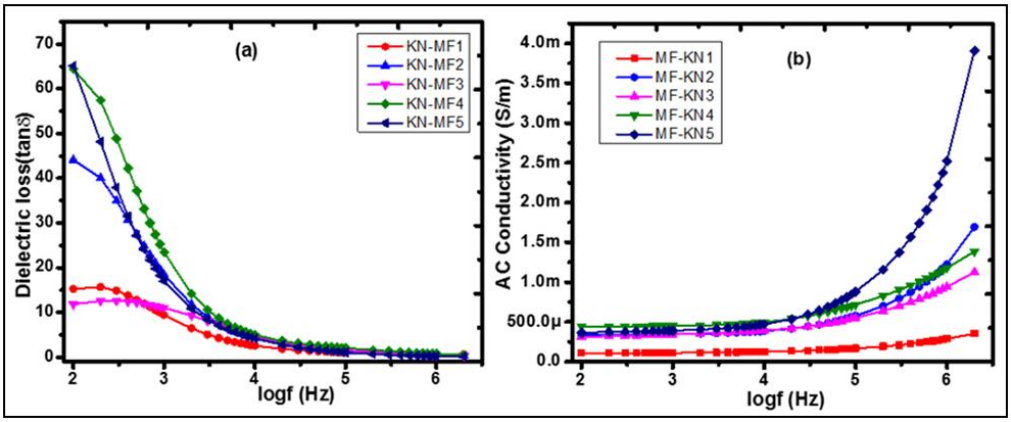

Figure 6. (a) Frequency dependence of dielectric loss and (b) Frequency dependence AC conductivity of (1-x)$KNbO_3$ - x$MgFe_2O_4$ mixed composites.

Figure 6(a) shows room temperature frequency dependence of loss ($tan\delta$) and figure (b) room temperature frequency dependence of AC conductivity (σ_{AC}) of (1-x)$KNbO_3$ - x$MgFe_2O_4$

mixed composites. Variation of dielectric loss ($tan\delta$) of the composites is proportional to ε' and ε'' which is the same trend (Ryu et al., 2001; Huang et al., 2016) high dielectric loss value at low frequency and low dielectric loss at high frequency with similar dispersion and vice versa as shown in figure 6(a). Dielectric loss variation with frequency attributed to domain wall resonance in low frequency region and inhibition of domain wall motion at high frequency region (Chen et al., 2018). The magnitude of the peak value of loss tangent decreases as ferrite content decreases in the composite. Loss tangent value measures electricl energy loss at different frequency. All the composites have very low loss tangent value at higher frequency region from all composites sample KN - MF1 has the lowest value. Loss tangent value of the composites show abnormal value due to changes of ferrite content in the composites which is collective behavior of charge carriers (Rahamann et al., 2014). A dielectric material with low loss tangent value at higher frequency means the material has a potential application in magnetically tunable filters, microwave devices and oscillators (Rezluscu et al., 1974).

Variation of AC conductivity (σ_{AC}) as a function of frequency is shown in figure 6(b). As it clearly seen the plots are nearly linear for famaller value of frequency indicating small dependence of AC conductivity. AC Conduction mechanisim of ferrite –ferroelectric composite is explained by polaron hopping (Adler et al., 1970) among localized states. The incorporation of ferrite material to ferroelectric material results an increase of σ_{AC} due to generation of charge carriers. At lower applied field frequency region resistive grain boundaries becomes more active consequently polaron hopping process becomes negligible. On the other hand, at higher applied field frequency region conductive phase becomes more active because hopping of charge carriers. Hopping of charges is restricted to the nearest site/inside the grain due to mismatch of the high frequency applied field and response time (Chen et al., 2018). This applied field frequency dependent AC conductivity attributed to small polaron type mechanism (Raveendran et al., 2019).

AC conductivity increases with an increase of ferrite content and the smallest value of the loss tangent is for the sample that has 50 % of $KNbO_3$ and 50% of $MgFe_2O_4$ compositions. Similarly this sample has largest dielectric constant.

In general, desirable properties of a dielectric material which include low dielectric loss tangent at high frequency and high permitivity that originate at interface were observed from all composite samples. The value for real permittivity, imaginary permitivity, loss tangent and AC

conductivity at 1 MHz applied electric field frequency of the composites are shown in table 3. As seen in the table AC conductivity of the ccomposite increases with the increase of ferrite content and the highest value of real permittivity and lowest value of loss tangent value is for sample KN-MF3 good for dielectric application.

Table 3. Value of real permittivity, imaginary permittivity, loss tangent and AC conductivity at 1 MHz applied field of (1-x)$KNbO_3$ - x$MgFe_2O_4$ mixed composites.

Composition (x)	***Real permitivity constant (ε')***	***Imaginary permitivity constant (ε'')***	***Loss tangent ($tan\delta$)***	***AC conductivity (σ_{AC})***
X=0.1	4.3 k	3.8 k	14.8	0.00032
X=0.3	1.39 k	60.5 k	43.8	0.0017
X=0.5	4.74 k	55. 5 k	11.5	0.0011
X=0.7	1.23 k	78. 9 k	64.2	0.0014
X=0.9	0.31 k	19.32 k	65.1	0.00392

3.3. Complex Impedance Spectra Analysis

Figure 7(a) show room temperature frequency dependence of real impedance (Z') and figure 7(b) room temperature frequency dependence of imaginary impedance (Z'') spectra of (1-x)$KNbO_3$ - x$MgFe_2O_4$ mixed composites. As seen in figure 7(a) real impedance (Z') of all the composites samples plot show a low-frequency dispersion and all merging at higher frequency with low value. This is because as applied field frequency increases conductivity becomes more active this may be related to charge ordering matter and mismatch of the response of electrons to applied field frequency.

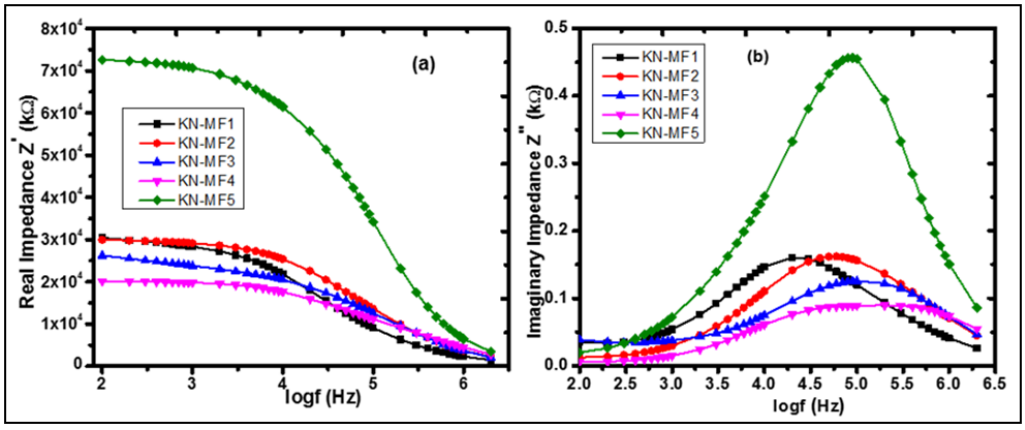

Figure 7. (a) Frequency dependence of real impedance and (b) frequency dependence of imaginary impedance of (1-x)$KNbO_3$ - x$MgFe_2O_4$ mixed composites.

As seen in figure 7(b) all composite samples plots show the same variation with frequency attaining different maximum values at different frequency and merging at a higher frequency. Imaginary dielectric constant Z'' peak frequency variation is due to the relaxation phenomenon (Devan et al., 2006). This merging of plots at a higher frequency attribute to the increase of conductivity at higher frequency. In both cases the merge of impedance value at at a higher frequency occurred this is due to the release of space charge carriers at the interface (Verma et al., 2012).

Figure 8 shows real impedance versus imaginary impedance (1-x)$KNbO_3$ - x$MgFe_2O_4$ mixed composites. As seen in figure 8 all plots of the composites are composed of different semicircles. These semicircle represent a distinct process with a different range of frequencies that demonstrate the existence of a good homogeneity of dielectric and conductive properties. Semicircle pattern change is with change of ferrite-ferroelectric composition which is an indication of modification of resistance – reactance amount in the composite. The observed semi-circles diameter variation resembles to the variation ferrite ferroelectric content (Chourashiya et al., 2008) which is dependent on the conduction mechanism of ferrite-ferroelectric content. Semi-circles at lower and higher frequency represent bulk condition process and electron transfer process and the intermediate frequencies represent the grain boundary condition of the respective samples (Ya et al., 2008).

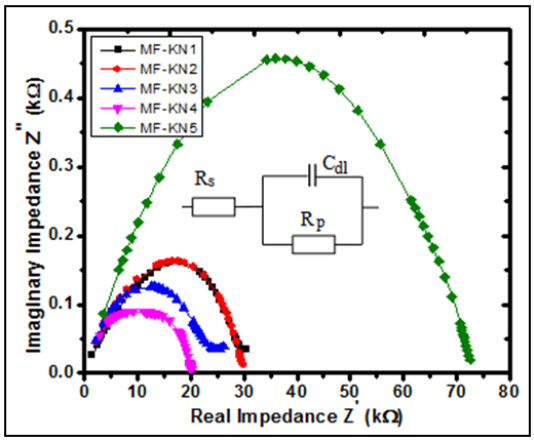

Figure 8. Complex impedance spectra (Nyquist plot) of (1-x)$KNbO_3$ - x$MgFe_2O_4$ mixed composites.

3.4. Magnetic Property Study

To study magnetic properties of the composites, room temperature VSM (Vibrating Spin Magnetometer) measurements were carriedout with maximum applied field of ± 3 kOe as shown

in figure 9. All the samples exhibit a magnetic hysteresis loop, which indicate the presence of orderd magnetic structure in the composites. and this confirm the presence of odered magnetic structure. Saturation magnetization of the composites increases with an increase of ferrite content from 0.04518 emu/g for KN-MF1 to 0.62976 emu/g for KN-MF5 (Mudinepalli et al., 2017). The steepest parts of magnetic hysteresis loops correspond to to the process of rotation in the spontaneous magnetization area (Kanamadi et al., 2009).

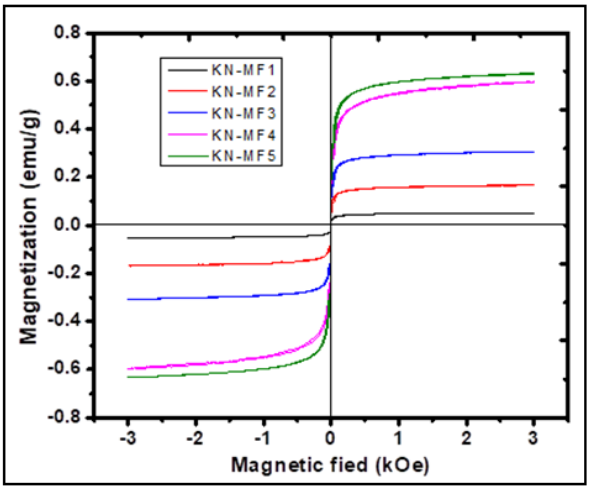

Figure 9. Complex impedance spectra of (1-x)$KNbO_3$ - x$MgFe_2O_4$ mixed composites.

3.4. ME Coupling Meaurements

Room-temperature magnetoelectric coupling measurments of (1-x)$KNbO_3$ - x$MgFe_2O_4$ (x = 0.1, 0.3, 0.5, 0.7, 0. 9) mixed composites have been investigated using a lock-in amplifier technique by varying applied AC magnetic field. The output ME voltage is measured at a fixed frequency of 850 Hz with a constant DC bias field of 2000 Oe collinearly with sweeping AC magnetic field varying from 0 to 90 Oe. Magnetoelectric coupling voltage calculated using the slope of the developed electric field across the samples versus the applied AC magnetic field. Magnetoelectric coupling response resulted from the appearance of electric polarization upon applying a magnetic field which increases with the an icrease of the applied AC magnetic field show linear dependence. Linear magnetoelectric coupling coefficient α_{ME} of the composite samples calculated from the slope of magnetoelectric coupling voltage versus applied AC magnetic field using the following relation (Verma et al., 2017):

$$\alpha_{ME} = \frac{\Delta V_{out}}{t \Delta H_{AC}} \quad (4)$$

Where, $V_{out}$is the output voltage, t sample/pellet thickness and H_{AC} the amplitude of the applied AC magnetic field.

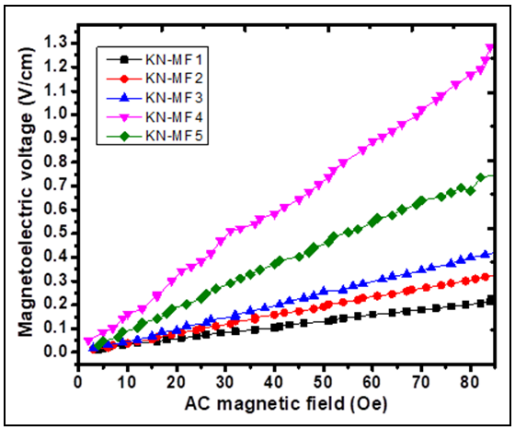

Figure 10. Magnetoelectric voltage with varying AC magnetic field (1-x)$KNbO_3$ - x$MgFe_2O_4$ mixed composites.

Figure 10 shows the magnetoelectric coupling response of (1-x)$KNbO_3$ - x$MgFe_2O_4$ (x = 0.1, 0.3, 0.5, 0.7, 0. 9) mixed composites with varying AC magnetic field at room temperature that shows dependence of ME coupling voltage with AC magnetic field. The calculated linear magnetoelectric coupling coefficient result reveals all composite samples exhibit ME coupling that increases with the increase of the applied magnetic field. ME response is found to be increasing in the composite with the increase of ferrite (Komalavalli et al., 2019) content this can be explained by the increase in the magnetostriction due to the substantial increase of the magnetostrictive phase (Mudinepalli et al., 2017). Magnetoelectrric effect of the composite is associated with the movement of magnetic domains in ferrite which are spontaneously deformed to the direction of magnetization that contributes to the increase of magnetostriction (Mudinepalli et al., 2015). In these composite materials, the coupling of ferrite and ferroelectricity is expected to originate at the interface between ferrite-ferroelectric phases (Nan et al., 2001; Thankachan et al., 2018).

Table 4. Magnetoelectric voltage coefficient, ferrite and ferroelectric contents of each sample.

Samples	***KN-MF1***	***KN-MF2***	***KN-MF3***	***KN-MF4***	***KN-MFN5***
Ferrite ($MgFe_2O_4$)	10 %	30 %	50 %	70 %	90 %
Ferroelectric $KNbO_3$	90 %	70 %	50 %	30 %	10 %
ME coefficient	2.6 mV/cmOe	3.8 mV/cmOe	4.9 mV/cmOe	15.5 mV/cmOe	9 mV/cmOe

Linear magnetoelectric coupling coefficient, α_{ME} value of all mixed composite samples are tabulated in table 4. Sample KN-MF4 has the highest magnetoelectric coupling value this makes it choosable for memory device application.

4. CONCLUSION

Multiferroic mixed composites were prepared from $MgFe_2O_4$ (MF) and potassium niobate (KN) with different molar ratio (1-x)$KNbO_3$ - x$MgFe_2O_4$ (x = 0.1, 0.3, 0.5, 0.7, 0. 9) using conventional solid state reaction method and the existence of the two ferrite/ferroelectric pure phases verified in all samples using XRD analysis. Morphology and microstructure of composite samples were studied using Images from TEM and HRTEM reveal the existence of two phases. Dielectric properties of the composite samples depend on ferrite content and dielectric dispersion at lower frequency is observed due to interfacial polarization. Low dielectric loss tangent at the high frequency of applied electric field and high dielectric constant that originate at the interface was observed. Maximum dielectric loss between 0.1 MHz and 1 MHz which is attributed to equal hopping frequency of electrons between different ionic states. The AC conductivity is related to the hopping of electrons and hopping conduction increases with frequency. Cole-Cole plots result demonstrate the formation of interfacial layer between $KNbO_3$ and $MgFe_2O_4$ grains and the reduction of the bulk resistance of the ferroelectric material with the increase of ferrite contents in mixed composites. Magnetic properties improved with addition of ferrite/ $MgFe_2O_4$ material . Increament of ME coupling coefficient with an increase of ferrite content. This composite material can be highly useful for the design of ultra-modern devices based on magnetoelectric multiferroics and microwaves.

5. ACKNOWLEDGEMENTS

The author (TkW) is thankful to Department of Science and Technology, New Delhi under the Nano Mission, PURSE, FIST Programs, International Inter-University Center For Nanoscience and Nanotechnology, MGU, Kottayam, Kerala, India.

6. REFERENCE

Abraham, A. R., Raneesh, B., Woldu, T., Aškrabić, S., Lazović, S., Mitrović, Z. D., Oluwafemi, O. S., Thomas, S & Kalarrikal, N. 2017. Realization of Enhanced magnetoelectric

Coupling and Raman Spectroscopy Signatures in 0-0 Type Hybrid Multiferroic core-Shell Geometric Nanostructures. *Journal of Physical Chemistry C*, **121**: 4352–4362.

Adler, D & Feinlein, J. 1970. Electrical and Optical Properties of Narrow Band Materials. *Physical Review B: Condensed Matter*, **2**: 3112-3134.

Chen, J., Wang, X & Pan, Z. 2018. High dielectric Constant and Low Dielectric Loss poly(vinylidene fluride) nanocomposites via a Small loading of Two – Dimentional Bi_2Te_3 @Al_2O_3 Hexagonal nanocomposite. *Journal of material Chemistry C*, **6**: 271-279.

Chourashiya, M. G., Patil, J. Y., Pawar, S. H & Jadhav, L. D. 2008. Studies on Structural, Morphological and Electrical Properties of $Ce_{(1-x)}Gd_x$ O_x $O_{2-x/2}$. *Materials Chemistry and Physics*, **109**: 39.

Corral, V., Bueno-Baques, D & Ziolo, R. F. 2010. Synthesis and Characterization of Novel $CoFe_2O_4$–$BaTiO_3$ Multiferroic Core-Shell Type Nanostructures. *Acta Materialia,* **58(3)**: 764-769.

Devan, R., Kanadimadi, C., Lokare, S & Chougule, B. K. 2006. Electrical Properties of Magnetoelectric Effect Measurement in Multiferroic $xNi_{0.8}Cu_{0.2}Fe_2O_4$–(1-x) $Ba_{0.9}Pb_{0.1}Ti_{0.9}Zr_{0.1}O_3$ Composites. *Smart Materials Structure*, **15**: 1877-1881.

Eerenstein, W., Mathur, N. D & Scott, J. F. 2006. Multiferroic and magnetoelectric. *Nature*, **442**: 759-765.

Fiebig, M. 2005. Revival of the Magnetoelectric Effect. *Journal of Physics*, **38**: R123-R152.

Giorgio Schileo, 2013. Recent Developments in Ceramic Multiferroic Composite Based on Core/Shell and Other Hetrostructures Obtained by Sol-gel routes. *Progress in Solid State Chemistry*, **41**: 87- 98.

Hill, Nicola A. 2000. Why Are Therere so Few Magnetic Ferroelectrics?. *Journal of Physical Chemistry*, B: **104**: 6694-6709.

Huang, B., Wang, B. Y., Du, Z. Y & Chen, X. M., 2016. Importing Spontaneous Polarization into a Heisenberg Ferromagnet for a Potential Single-phase Multiferroic. *Journal of Materials Chemistry C*, **4**: 8704-8710.

Islam, R. A., Bedekar, V., Poudyal, N., Ping, J. L & Priya, S. J. 2008. Magnetoelectric properties of core-shell particulate nanocomposites. *Journal of Applied Physics*, **104(10)**: 104111 (1-5).

Kanamadi, C. M., Kim, J. S., Yang, H. K., Moon, B. K., Choi, B. C & Jeong, J. H. 2009. Structural, Magnetic and Electrical Properties of Barium Titanate and Magnesium Ferrite Composites. *Journal of Alloys and Compounds*, **481**: 781-785.

Kim, T. Y., Song, S., Jang, H. M., Peters, J. A & Jeong, Y. K. 2014. Controllable Magnetic Anisotropy of Ferromagnet/antiferromagnet Bilayers Coupled with Piezoelectric Strain. *Journal of Matertairial Chemistry* C, **2**: 8018-8022.

Komalavalli, P., Shameen banu, I. B & Shahid Anwar, M. 2019. Magnetoelectric Coupling of Manganese Ferrite-Potassium Niobate Lead-Free Composite Ceramics Synthesizad by Solid State Reaction method. *Journal of Materials Science: Materials in Electronics* **30**: 3411-3417.

Koo, Y. S., Song, K. M., Nur, N., Jung, J. H., Jang, T. H., Lee, H. J., Koo, T. Y., Jeong, Y. H., Cho, J. H & Jo, Y. H. 2009. Functional Properties of $BaTiO_3$ – $Ni_{0.5}ZN_{0.5}Fe_2O_4BaTiO_3$ - $Ni_{0.5}ZN_{0.5}Fe_2O_4$ Magnetoelectric Coupling Prepqred from powders with core-shell Structure. *Applied Physics Letter*, **94**: 032903.

Koops, C. G. 1951. On the Dispersion of Resistivity and Dielectrc Constant of Some semiconductors at Audio frequencies. *Physical Review*, **83**: 121-128.

Liu, Y., Wu, Y., Li, D., Zhang, Y & Yang, J. 2013. A study of Structural, Ferroelectric, Ferromagnetic, Dielectric Properties of $NiFe_2O_4$–$BaTiO_3$ Multiferroic Composites .*Journal of Material Science: Materials in Electronics*, **24**: 1900-1904.

Mudinepalli, V. R., Feng L., Lin W. C. & Murty B. S. 2015. Effect of grain size on dielectric and ferroelectric properties of nanostructured $Ba_{0.8}Sr_{0.2}TiO_3$ ceramics. *Journal of Advanced Ceramics*, **4**(1):46-53.

Mudinepalli, V. R., Song, S. H., Li, Q & Murthy, S. 2017. Magnetoelectric Coupling of manganese Ferrite-potassium Niobate Lead-Free Composite Ceramics Synthesized by Solid State Reaction Method. *Journal of Magnetism and Magnetic Materials*, **386**: 44-49.

Nan, C. W., Bichrin, M. I., Dong, S. X., Viehland, D & Srinivasan, G. 2008. Multiferroic Magnetoelectric Composites: Historical Perspective. *Journal of Applied Physics*, **103**: 031101-35.

Nan, C. W., Li, M & Haung, J. H. 2001. Calculations of giant magnetoelectric effects in ferroic composites of rare-earth–iron alloys and ferroelectric polymers. *Physical Review B: Condensed Matter*, **63**: 144415.

Nayek, C., Sahoo, K. K & Murugavel, P. 2013. Magnetoelectric Effect in $La_{0.7}Sr_{0.3}MnO_3$ – $BaTiO_3$ Core–Shell Nanocomposite. *Mater Res Bull*, **48**: 1308–1311.

Pandya, R. J., Joshi, U. S & Caltun, O. F 2015. Microstructural and Electrical Properties of Barium Storium Titanate and Nickel Zinc Ferrite Composites. *Procedia Materials Science*, **10**: 168-175.

Park, J. H., kim, M., Ahn, S. J., Ryu, S & Jang, H. M. 2009. Interfacial Strain-Mediated magnetoelectric coupling as Reflected in Extended X-Ray absorption spectra of $coFe_2O_4$ dipersed Pb(Zr, Ti)O_3 Matix Composites. *Journal of Magnetism and Magnetic Materials*, **321**: 1971-1974.

Pascual-Gonzalez, C., Schileo, G & Feteira, A. 2016. Continiously Controlable Optical band Gap in Orthorhombic Ferroelectric $KNbO_3$-$BiFeO_3$ ceramics. *Applied Physics Letter*, **109**: 132902.

Petrov, V. M., Srinivasan, G., Bichurin, M. I & Gupta, A. 2007. Theory of Magnetoelectric Effects in Piezoelectric Nanocomposites. *Physical Review* B, **75**: 224407.

Quittet, A. M, Bell, M. I., Krauzman, M & Raccah, P. M. 1976. Anomalous scattering and asymmetrical line shapes in Raman spectra of orthorhombic KNbO3. Physical Review B **14**: 5068.

Rahamann, Md. D., Saha, S. K., Ahmed, T. N., Saha, D. K & Akther Hossain, A. K. M. 2014. Phase Transformation, Nanorod-like Morphology, Wide bandgap, and Dieectric properties of (1-x) $Al_{0.2}La_{0.8}TiO_3$ - x$BaTiO_3$ Nanocomposites. *Journal of Magnetism Magnetic Materials*, **371**: 112-120.

Raidongia, K., Nag, A., Sundaresan, A & Rao, C. N. 2010. Multiferroic and Magnetoelectric Coupling Properties of $CoFe_2O_4$–$BaTiO_3$ Nanocomposites. *Applied Physics Letters*, **97**: 062904.

Ramesh, R & Spaladin, N. A. 2007. Multiferroics: Progress and Prospects in Thin Films. *Nature Materials*, **6**: 21-29.

Ramesh, T., Rajendar, V & Murthy, S. R. 2017. $CoFe_2O_4$–$BaTiO_3$ Multiferroic Composites: Role of Ferrite and Ferroelectric Phases on the Structural, Magneto Dielectric Properties. *Journal of Material Science: Materials in Electronics*, **28**: 11779-11788.

Raneesh, B., Nandakumar, K., Saha, D. Das, Soumya, H., Philip, J & Philip, R. 2015. Composition structure-physical property relationship and nonlinear optical properties of

multiferroic hexagonal $ErMn_{1-x}Cr_xO_3$ nanoparticles. *Royal Socitey of Chemistry*, **5**: 12480 -12487.

Rani, J., Yadav, K. L & Prakash , S. 2014. Enhanced Magnetoelectric Effect and Optical Propertes of Lead Free Multiferroic $(1-x)Bi_{0.5}Na_{0.5}TiO_3 – xCoFe_2O_4$. *Materials Chemistry and Physics*, **147**: 1183-1190.

Raveendran, A., Sebastian, M. T & Raman, S. 2019. Applications Of Macrowave Materials: A Review. *Journal of Electronic Materials,* **48(5)**: 2601-2634, DOI:10.1007/s11664-019-07049-1.

Rezluscu, N & Rezluscu, E. 1974. Diectric Properties of Copper Containing Ferrites. *Solid State Physics*, **23(2)**: 575-582, https://doi.org/10.1002/pssa.2210230229.

Ryu, J., Carazo, A.Z., Uchino, K & Kim, H. E. 2001. Piezoelectric and Magnetoelectric properties of Lead Zirconate Titanate/Ni-ferrite Particulate composites. *Journal of Electroceramic*, **7**: 17-24.

Sadhana, K. Murthy, S.R., Jie, S., Xie, Y., Liu, Y., Zhan, Q & Li, R.W. 2013. Magnetic Field Induced Polarization and Magnetoelectric Effect of $Ba_{0.8}Ca_{0.2}TiO_3– Ni_{0.2}Cu_{0.3}ZN_{0.5}Fe_2O_4$. *Journal of Applied Physics*, **113**: 17C731.

Shen, Z. X., Hu, Z. P., Chomg, T. C., Beh, C. Y., Tang, S. H & Kuok, M. H. 1995. Pressure-induced Strong mode Coupling and Phase Transition in $KNbO_3$. *Physical Review B 52*, **6**: 3976.

Spaladin, N. A & Fiebig, M. 2005. The Renaisanceof magnetoelectric Multiferroics. *Science*, **309**: 391–392.

Tan, S. Y., Shannigrahi, S. R., Tan, S. H & Tay, F. E. H. 2008. Synthesis and Characterization of Composite $MgFe_2O_4–BaTiO_3$ Multiferroic System. *Journal of Applied Physics*, **103**: 094105.

Thankachan, R. M., Raneech, B., Mayeen, A., Karthika, S., Vivek, S., Nair, S. S., Thomas, S & Kalarikkal, N. 2018. Room Temperature Magnetoelectric Coupling Effect in $CuFe_2O_4$ /$BaTiO_3$ Core-Shell and Mixed nanocomposites. *J. Alloy and Compounds*, **15**: 288-296.

Vaz, C. A. F., Hoffman, J. , Ahn, C. H & Ramesh, R. 2010. Magnetoelectric Coupling Effect in Multiferroic complex Oxide Composite structures. *Advanced Materials*, **22**: 2900.

Verma, K & Sharma, S. 2012. Impedance Spectroscopy and Dielectric Behavior in Barium Storium Titanate – Nickel – Zinc Ferrite Composites. *Basic Solid State Physics*, **249(1)**: 209-216.

Verma, K. C., Singh, D., Kumar, S & Kontala, R. K. 2017. Multiferroic Effects in M Fe_2O_4 /$BaTiO_3$ (M=Mn, Co, Ni, Zn) Nanocomposites. *J. Alloys and Compounds*, **709**: 344-355.

Wagner, K. W. 1993. The Distribution of Relaxation Times in Typical dielectrics. *Annual Physics*, **40**: 818-826.

Wang, Z., Lazor, P., Saxena, S. K & O'Niel, Hugo St. C. 2002. High Pressure Raman Spectroscopy of Ferrite $MgFe_2O_4$. *Material Research Bulletin*, **37**: 1589-1602.

Wang, K. F., Liu. J. M & Ren, Z. F. 2009. Multiferroicity: The Coupling Between Magnetic and Polarization Orders. *Advanced Physics*, **58**: 321–448.

Xie, S. H., Ma, F. Y., Liu, Y. M & Li, J. Y. 2011. Multiferroic $CoFe_2O_4$–$Pb(Zr_{0.52}Ti_{0.48})O_3$ Core-Shell nanofibers abd their Magnetoelectric Coupling. *Nanoscale*, **3**: 3152.

Ya, H., Jackman, R.B & Hing, P. 2008. Electrical Properties of Aggregated detonation nanodiamonds. *J ournal of Applied Physics*, **94**: 7878.

Zhai, J. Y., Xing, Z. P., Dong, S. X., Li, J. F & Viehland, D. 2008. Magnetoelectric Laminate Composites: An Over view. *Journal of American Ceramics Socitey*, **91**: 351.

Zhao, Y., Miao, J., Meng, X. B., Weng, F., Xu, X. G., Jiang, Y & Wang, S. G. 2014. Butterfly-Shaped Multiferroic $BiFeO_3$@$BaTiO_3$ Core-Shell Nanotubes: The Interesting Structural Multiferroic, and Optical Properties. *Journal of Material Science: Materials in Electronics*, **24**: 1439–1445.

Zhu, Q., Xie, Y & Zhang, J. 2014. Multiferroic $CoFe_2O_4$–$BiFeO_3$ Core-Shell Nanofibers and their Nanoscale Magnetoelectric Coupling. *Journal of Material Research*, **29**: 657-664.